

Nucleon Resonance Excitation with Virtual Photons

L. Tiator* and S. Kamalov†

**Institut für Kernphysik, Universität Mainz, 55099 Mainz, Germany*

†*JINR Dubna, 141980 Moscow Region, Russia*

Abstract. The unitary isobar model MAID is used for a partial wave analysis of pion photoproduction and electroproduction data on the nucleon. In particular we have taken emphasis on the region of the $\Delta(1232)$ resonance and have separated the resonance and background amplitudes with the K-matrix approach. This leads to electromagnetic properties of the dressed Δ resonance, where all multipole amplitudes become purely imaginary and all form factors and helicity amplitudes become purely real at the K-matrix pole of $W = M_\Delta = 1232$ MeV. The $R_{EM} = E2/M1$ and $R_{SM} = C2/M1$ ratios of the quadrupole excitation are compared to recent data analysis of different groups. The R_{EM} ratio of MAID2005 agrees very well with the data and has a linear behavior over the whole experimentally explored Q^2 region with a small positive slope that predicts a zero crossing around 3.5 GeV^2 . The recent R_{SM} data for $Q^2 < 0.2 \text{ GeV}^2$ indicate a qualitative change in the shape of the ratio which can be explained by the impact of the Siegert theorem at pseudothreshold ($Q^2 = -0.086 \text{ GeV}^2$) in the unphysical region.

Keywords: Partial-Wave Analysis, Pion Electroproduction, Transition Form Factors, Helicity Amplitudes

PACS: 13.40.Gp, 14.20.Gk, 11.80.Et, 13.30.Eg

INTRODUCTION

Our knowledge of nucleon resonances is mostly given by elastic pion nucleon scattering [1]. All resonances that are given in the Particle Data Tables [2] have been identified in partial wave analyses of πN scattering both with Breit-Wigner analyses and with speed-plot techniques. From these analyses we know very well the masses, widths and the branching ratios into the πN and $\pi\pi N$ channels. These are reliable parameters for all resonances in the 3- and 4-star categories. There remain some doubts for the two prominent resonances, the Roper $P_{11}(1440)$ which appears unusually broad and the $S_{11}(1535)$ that cannot uniquely be determined in the speed-plot due to its position close to the ηN threshold. As an alternative to the quark model, these resonances can also be generated with dynamical methods [3, 4, 5]. On the other hand attempts have been made to calculate nucleon resonances in quenched QCD on the lattice [6], and in the case of the $\Delta(1232)$ even the transition form factors are evaluated on the lattice [7].

Starting from these firm grounds, using pion photo- and electroproduction we can determine the electromagnetic γNN^* couplings. They can be given in terms of electric, magnetic and charge transition form factors $G_E^*(Q^2)$, $G_M^*(Q^2)$ and $G_C^*(Q^2)$ or by linear combinations as helicity amplitudes $A_{1/2}(Q^2)$, $A_{3/2}(Q^2)$ and $S_{1/2}(Q^2)$. So far, we have some reasonable knowledge of the $A_{1/2}$ and $A_{3/2}$ amplitudes at $Q^2 = 0$, which are tabulated in the Particle Data Tables. For finite Q^2 the information found in the literature is very scarce and practically does not exist at all for the longitudinal amplitudes $S_{1/2}$. But even for the transverse amplitudes only few results are firm, these are the G_M^* form factor of the $\Delta(1232)$ up to $Q^2 \approx 10 \text{ GeV}^2$, the $A_{1/2}(Q^2)$ of the $S_{11}(1535)$ resonance up to $Q^2 \approx 5 \text{ GeV}^2$ and the helicity asymmetry $A_1(Q^2)$ for the $D_{13}(1520)$ and $F_{15}(1680)$ resonance excitation up to $Q^2 \approx 3 \text{ GeV}^2$ which change rapidly between -1 and $+1$ at small $Q^2 \approx 0.5 \text{ GeV}^2$ [8]. Frequently also data points for other resonance amplitudes, e.g. for the Roper are shown together with quark model calculations but they are not very reliable. Their statistical errors are often quite large but in most cases the model dependence is as large as the absolute value of the data points. In this context it is worth noting that also the word ‘data point’ is somewhat misleading because these photon couplings and amplitudes cannot be measured directly but can only be derived in a partial wave analysis. Only in the case of the $\Delta(1232)$ resonance this can and has been done directly in the experiment by Beck et al. at Mainz [9]. For the Delta it becomes possible due to two important theoretical facts, the Watson theorem and the well confirmed validity of the $s+p$ – wave truncation. Within this assumption a complete experiment was done with polarized photons and with the measurement of both π^0 and π^+ in the final state, allowing also for an isospin separation. For other resonances neither the theoretical constraints are still valid nor are we any close to a complete experiment. The old data base was rather limited with large error bars and no data with either target or recoil polarization was available. Even now we do not have many data points with

double polarization, however, the situation for unpolarized $e + p \rightarrow e' + p + \pi^0$ has considerably improved, mainly by the new JLab experiments in all three halls A, B and C. Furthermore electron beam polarization has been used in a couple of experiments at Mainz, Bates and JLab. These data cover a large energy range from the Delta up to the third resonance region with a wide angular range in θ_π . Due to the 2π coverage in the ϕ angle, a separation of the unpolarized cross section

$$\frac{d\sigma_v}{d\Omega} = \frac{d\sigma_T}{d\Omega} + \varepsilon \frac{d\sigma_L}{d\Omega} + \sqrt{2\varepsilon(1+\varepsilon)} \frac{d\sigma_{LT}}{d\Omega} \cos\phi + \varepsilon \frac{d\sigma_{TT}}{d\Omega} \cos 2\phi + h\sqrt{2\varepsilon(1-\varepsilon)} \frac{d\sigma_{LT'}}{d\Omega} \sin\phi \quad (1)$$

in four parts becomes possible and is very helpful for the partial wave analysis. Even without a Rosenbluth separation of $d\sigma_T$ and $d\sigma_L$ we have an enhanced sensitivity of the longitudinal amplitudes due to the $d\sigma_{LT}$ and $d\sigma_{LT'}$ interference terms. Such data are the basis of our new partial wave analysis with an improved version of the Mainz unitary isobar model MAID.

THE DYNAMICAL APPROACH TO MESON ELECTROPRODUCTION

In the dynamical approach to pion photo- and electroproduction [10, 11, 12], the t-matrix is expressed as

$$t_{\gamma\pi}(E) = v_{\gamma\pi} + v_{\gamma\pi} g_0(E) t_{\pi N}(E), \quad (2)$$

where $v_{\gamma\pi}$ is the transition potential for $\gamma^* N \rightarrow \pi N$, and $t_{\pi N}$ and g_0 denote the πN t-matrix and free propagator, respectively, with $E \equiv W$ the total energy in the c.m. frame. A multipole decomposition of Eq. (2) gives the physical amplitude

$$t_{\gamma\pi}^\alpha(q, k; E + i\varepsilon) = \exp(i\delta^\alpha) \cos\delta^\alpha \left[v_{\gamma\pi}^\alpha(q, k) + P \int_0^\infty dq' \frac{q'^2 R_{\pi N}^\alpha(q, q'; E) v_{\gamma\pi}^\alpha(q', k)}{E - E_{\pi N}(q')} \right], \quad (3)$$

where δ^α and $R_{\pi N}^\alpha$ are the πN scattering phase shift and reaction matrix in channel α , respectively; q is the pion on-shell momentum and k is the virtual photon momentum for a four-momentum transfer of $-Q^2$,

$$q = \frac{\sqrt{(W^2 - (M_N + m_\pi)^2)(W^2 - (M_N - m_\pi)^2)}}{2W}, \quad k = \frac{\sqrt{(Q^2 + (W + M_N)^2)(Q^2 + (W - M_N)^2)}}{2W}.$$

For simplicity we give here the expressions which are strictly valid only in the limit of the Watson theorem. They are exact for the $\Delta(1232)$ but need to be modified for other resonances as discussed in detail in Ref. [13].

The multipole amplitude in Eq. (3) manifestly satisfies the Watson theorem and shows that the γ, π multipoles depend on the half-off-shell behavior of the πN interaction.

In a resonant channel the transition potential $v_{\gamma\pi}^\alpha$ consists of two terms

$$v_{\gamma\pi}^\alpha(W, Q^2) = v_{\gamma\pi}^{B,\alpha}(W, Q^2) + v_{\gamma\pi}^{R,\alpha}(W, Q^2), \quad (4)$$

where $v_{\gamma\pi}^{B,\alpha}(W, Q^2)$ is the background transition potential and $v_{\gamma\pi}^{R,\alpha}(W, Q^2)$ corresponds to the contribution of the bare resonance excitation. The resulting t-matrix can be decomposed into two terms

$$t_{\gamma\pi}^\alpha(W, Q^2) = t_{\gamma\pi}^{B,\alpha}(W, Q^2) + t_{\gamma\pi}^{R,\alpha}(W, Q^2). \quad (5)$$

The background potential $v_{\gamma\pi}^{B,\alpha}(W, Q^2)$ is described by Born terms obtained with an energy dependent mixing of pseudovector-pseudoscalar πNN coupling and t-channel vector meson exchanges. The mixing parameters and coupling constants were determined from an analysis of nonresonant multipoles in the appropriate energy regions. In the new version of MAID, the S, P, D and F waves of the background contributions are unitarized in accordance with the K-matrix approximation,

$$t_{\gamma\pi}^{B,\alpha}(\text{MAID}) = \exp(i\delta^\alpha) \cos\delta^\alpha v_{\gamma\pi}^{B,\alpha}(W, Q^2). \quad (6)$$

From Eqs. (3) and (6), one finds that the difference between the background terms of MAID and of the dynamical model is that off-shell rescattering contributions (principal value integral) are not included in MAID, therefore, after re-fitting the data, they are implicitly contained in the resonance part leading to dressed resonances.

Following Ref. [14], we assume a Breit-Wigner form for the resonance contribution of the *e.m.* multipoles $\mathcal{A}_\alpha^R(W, Q^2)$, which are the partial waves of the T-matrix $t_{\gamma\pi}^{R,\alpha}(W, Q^2)$ in Eq. (5),

$$\mathcal{A}_\alpha^R(W, Q^2) = \bar{\mathcal{A}}_\alpha^R(Q^2) \frac{f_{\gamma R}(W)\Gamma_R(W)M_R f_{\pi R}(W)c_{\pi R}}{M_R^2 - W^2 - iM_R\Gamma_R(W)} e^{i\phi(W)}, \quad (7)$$

where $f_{\pi R}$ is the usual Breit-Wigner factor describing the decay of a resonance R with total width $\Gamma_R(W)$ and physical mass M_R . The expressions for $f_{\gamma R}$, $f_{\pi R}$ and Γ_R are given in Ref. [14]. The factor $c_{\pi R}$ is $\sqrt{3/2}$ and $-1/\sqrt{3}$ for resonances with isospin 3/2 and isospin 1/2, respectively. The phase $\phi(W)$ in Eq. (7) is introduced to adjust the phase of the total multipole to equal the corresponding πN phase shift δ^α . While in the original version of MAID only the 7 most important nucleon resonances were included with mostly only transverse e.m. couplings, from version MAID2003 on all four star resonances below $W = 2$ GeV are included. These are $P_{33}(1232)$, $P_{11}(1440)$, $D_{13}(1520)$, $S_{11}(1535)$, $S_{31}(1620)$, $S_{11}(1650)$, $D_{15}(1675)$, $F_{15}(1680)$, $D_{33}(1700)$, $P_{13}(1720)$, $F_{35}(1905)$, $P_{31}(1910)$ and $F_{37}(1950)$.

The resonance couplings $\bar{\mathcal{A}}_\alpha^R(Q^2)$ can be taken as constants in a single- Q^2 analysis, e.g. in photoproduction, where $Q^2 = 0$ but also at any fixed Q^2 , where enough data with W and θ variation is available. Alternatively they can also be parametrized as functions of Q^2 . Then it is possible to determine the values $\bar{\mathcal{A}}_\alpha^R(0)$ from a fit to the world database of photoproduction, while the parameters of the Q^2 evolution can be obtained from a combined fitting of all electroproduction data at different Q^2 . The latter procedure we call the ‘superglobal fit’. In MAID the photon couplings $\bar{\mathcal{A}}_\alpha^R$ are input parameters. They are directly related to the helicity couplings $A_{1/2}, A_{3/2}$ and $S_{1/2}$ of nucleon resonance excitation as described later in the text.

PARTIAL WAVE ANALYSIS

The unitary isobar model MAID was used to analyze the world data of pion photo- and electroproduction. In a first step we have fitted the background parameters of MAID and the transverse normalization constants $\bar{\mathcal{A}}_\alpha^R(0)$ for the nucleon resonance excitation. The latter ones give rise to the helicity couplings. Most of the couplings are in good agreement with PDG and the GW/SAID analysis.

In Fig. 1 and Fig. 2 we give a comparison between MAID and SAID for four important multipoles, $M_{1+}(P_{33}), E_{1+}(P_{33}), E_{0+}(S_{11})$ and $E_{2-}(D_{13})$. For both analyses we show the global (energy dependent) curves together with the local (single energy) fits, where only data in energy bins of 10-20 MeV are fitted. Such a comparison demonstrates the fluctuations due to a limited data base or due to a weak sensitivity of the available data to a small multipole, e.g. in the case of the E_{0+} or E_{1+} multipoles. The very large efforts that had been made at MAMI and LEGS in the 90s to precisely determine the E/M ratio shows up with much better data points for E_{1+} around the Delta resonance position. Fig. 2 also shows systematic differences between the MAID and SAID analyses in the real parts of E_{0+} and E_{2-} . Due to correlations between these amplitudes, the differences cannot be resolved with our current data base. Because of isospin 1/2, they can, however, lead to sizeable differences in the γ, π^+ channel, where the data base is still quite limited.

In a second step we have fitted recent differential cross section data on $p(e, e'p)\pi^0$ from Mainz [15], Bates [16], Bonn [17] and JLab [18, 19, 20]. These data cover a Q^2 range from 0.1...4.0 GeV² and an energy range 1.1 GeV $< W < 2.0$ GeV. In a first attempt we have fitted each data set at a constant Q^2 value separately. This is similar to a partial wave analysis of pion photoproduction and only requires additional longitudinal couplings for all the resonances. The Q^2 evolution of the background is described with nucleon Sachs form factors in the case of the $s-$ and $u-$ channel nucleon pole terms. At the e.m. vertices of the π pole and seagull terms we apply the pion and axial form factors, respectively, while a standard dipole form factor is used for the vector meson exchange. Furthermore, as mentioned above, we have introduced a Q^2 evolution of the transition form factors of the nucleon to N^* and Δ resonances and have parameterized each of the transverse $A_{1/2}$ and $A_{3/2}$ and longitudinal $S_{1/2}$ helicity couplings. In a combined fit with all electroproduction data from the world data base of GWU/SAID [21] and the data of our single- Q^2 fit we obtained a Q^2 dependent solution (superglobal fit).

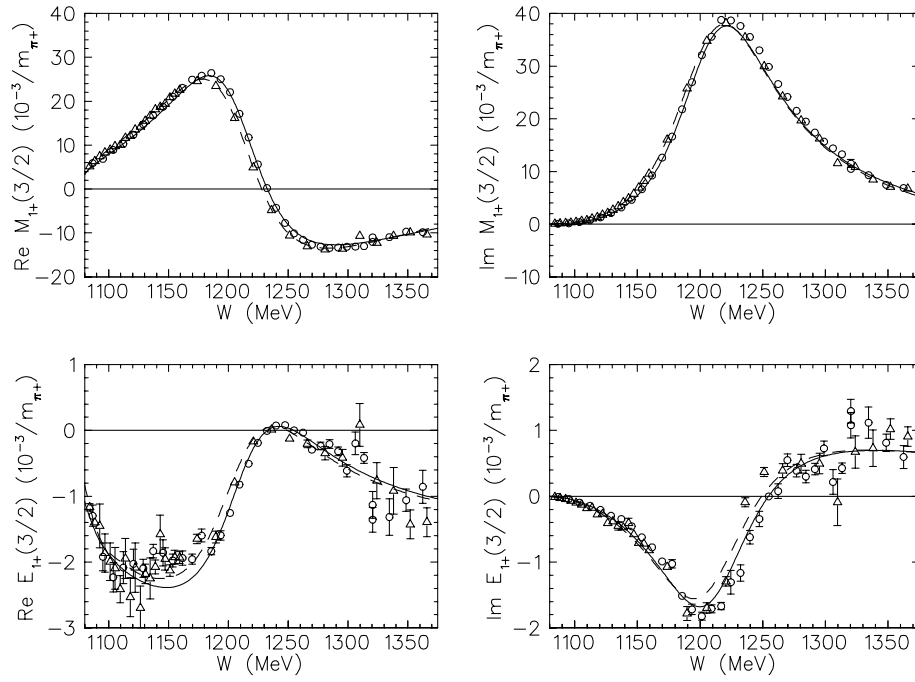


FIGURE 1. Real and imaginary parts of the P_{33} multipoles M_{1+} and E_{1+} . Our solution MAID05 (solid curve) is compared to the GW/SAID solution SM02 (dashed curve). The single-energy solutions (data points) are from MAID (open circles) and SAID (open triangles).

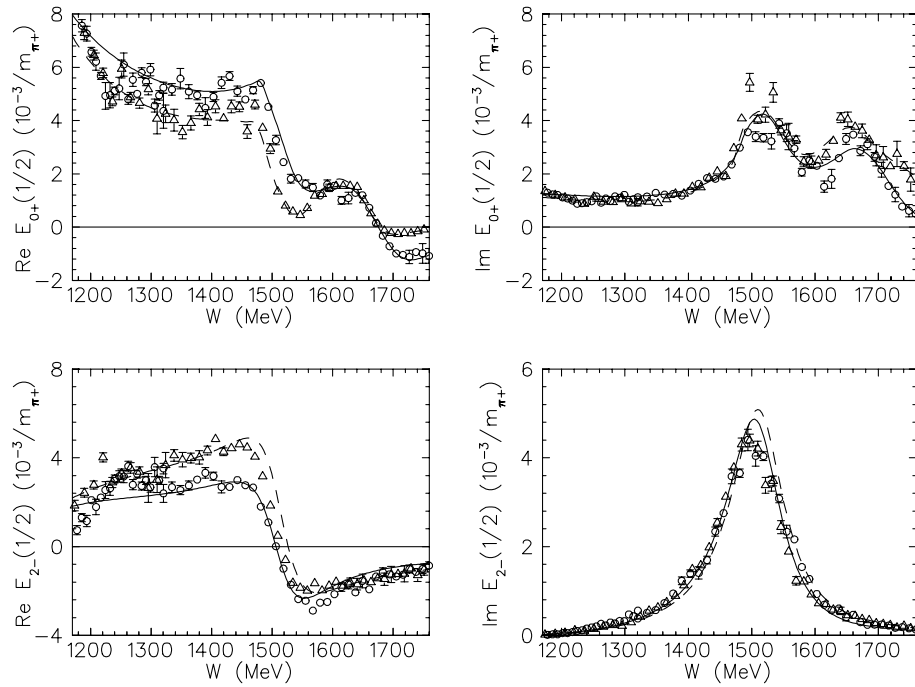


FIGURE 2. Real and imaginary parts of the S_{11} multipole E_{0+} and the D_{13} multipole E_{2-} . Notation as in Fig. 1

THE NUCLEON TO DELTA(1232) TRANSITION

For the resonance couplings of the P_{33} multipoles we find a convenient parametrization in the following form

$$\bar{\mathcal{A}}_{\alpha}^{\Delta}(Q^2) = \bar{\mathcal{A}}_{\alpha}^{\Delta}(0) \frac{k(W, Q^2)}{k(W, 0)} (1 + \beta_{\alpha} Q^{n_{\alpha}}) e^{-\gamma Q^2} G_D(Q^2) \quad (8)$$

with the usual dipole form factor $G_D(Q^2) = 1/(1 + Q^2/0.71 \text{ GeV}^2)^2$. Even though the exponential does not lead to the proper asymptotic behaviour of the helicity amplitudes, by this ansatz we get a much simpler parametrization which is well behaved in the physical region. On the other hand, the asymptotic behavior as predicted by pQCD is yet far outside of the currently accessible experimental range. The fitted parameters are listed in Table 1.

TABLE 1. Parametrization of the Q^2 dependence for the electromagnetic $N \rightarrow \Delta$ amplitudes. All 3 amplitudes have the same exponential factor with $\gamma = 0.21 \text{ GeV}^{-2}$ and $G_D(Q^2)$ is the dipole form factor $1/(1 + Q^2/0.71 \text{ GeV}^2)^2$.

	$\bar{\mathcal{A}}_{\alpha}^{\Delta}(0) (10^{-3} \text{ GeV}^{-1/2})$	n_{α}	$\beta_{\alpha} (\text{GeV}^{-n_{\alpha}})$
M1	294.	2	0
E2	-6.37	2	-0.31
C2	-19.5	6	0.0167

With the definition of Eq. (6), the background amplitudes of the P_{33} channel vanish exactly at the resonance position and the resonance amplitudes become purely imaginary. In this case the helicity amplitudes $A_{1/2}, A_{3/2}, S_{1/2}$, which are the characteristic numbers for *e.m.* resonance excitation, are directly related to the resonance multipoles at $W = M_{\Delta}$ (see e.g. PDG94 or Ref. [22]),

$$\begin{aligned} A_{1/2} &= -\frac{1}{2}(\bar{M}_{1+}^{(3/2)} + 3\bar{E}_{1+}^{(3/2)}), \\ A_{3/2} &= -\frac{\sqrt{3}}{2}(\bar{M}_{1+}^{(3/2)} - \bar{E}_{1+}^{(3/2)}), \\ S_{1/2} &= -\sqrt{2}\bar{S}_{1+}^{(3/2)} \\ \text{with } \{\bar{M}, \bar{E}, \bar{S}\}_{1+}^{(3/2)} &= \left(\frac{8\pi q_{\Delta} M_{\Delta} \Gamma_{\Delta}}{3k_W M_N} \right)^{1/2} \text{Im}\{M, E, S\}_{1+}^{(3/2)}(W = M_{\Delta}). \end{aligned} \quad (9)$$

In MAID these reduced resonance multipoles are identical to $\bar{\mathcal{A}}_{\alpha}^{\Delta}(Q^2)$. Using this definition we can now also define the $N \rightarrow \Delta$ transition form factors

$$\begin{aligned} G_M^*(Q^2) &= b_{\Delta} \bar{M}_{1+}^{(3/2)}(Q^2) = b_{\Delta} \bar{\mathcal{A}}_M^{\Delta}(Q^2), \\ G_E^*(Q^2) &= -b_{\Delta} \bar{E}_{1+}^{(3/2)}(Q^2) = -b_{\Delta} \bar{\mathcal{A}}_E^{\Delta}(Q^2), \\ G_C^*(Q^2) &= -b_{\Delta} \frac{2M_{\Delta}}{k_{\Delta}} \bar{S}_{1+}^{(3/2)}(Q^2) = -b_{\Delta} \frac{2M_{\Delta}}{k_{\Delta}} \bar{\mathcal{A}}_C^{\Delta}(Q^2) \\ \text{with } b_{\Delta} &= \left(\frac{8M_N^2 q_{\Delta} \Gamma_{\Delta}}{3\alpha_{em} k_{\Delta}^2} \right)^{1/2}, \end{aligned} \quad (10)$$

$\alpha_{em} = 1/137$, $\Gamma_{\Delta} = 115 \text{ MeV}$ and k_{Δ}, q_{Δ} the photon and pion momenta at $W = M_{\Delta}$. Eq. (10) corresponds to the definition of Ash [23], the form factors of Jones and Scadron [24] are obtained by multiplication with an additional factor, $G^{JS} = \sqrt{1 + Q^2/(M_N + M_{\Delta})^2} G^{Ash}$.

The *e.m.* transition form factors may also be expressed in terms of the helicity amplitudes $A_{1/2}, A_{3/2}$ and $S_{1/2}$, which are determined at the resonance position $W = M_{\Delta}$ and are functions of Q^2 ,

$$\begin{aligned} G_M^* &= -c_{\Delta}(A_{1/2} + \sqrt{3}A_{3/2}), \\ G_E^* &= c_{\Delta}(A_{1/2} - \frac{1}{\sqrt{3}}A_{3/2}), \end{aligned}$$

$$G_C^* = \sqrt{2}c_\Delta \frac{2M_\Delta}{k_\Delta} S_{1/2},$$

$$\text{with } c_\Delta = \left(\frac{m^3 k_W}{4\pi\alpha M_\Delta k_\Delta^2} \right)^{1/2} \quad (11)$$

and the equivalent photon energy $k_W = k(W, Q^2 = 0)$. The E/M and S/M ratios can then be defined as

$$R_{EM} = -\frac{G_E^*}{G_M^*} = \frac{A_{1/2} - \frac{1}{\sqrt{3}}A_{3/2}}{A_{1/2} + \sqrt{3}A_{3/2}},$$

$$R_{SM} = -\frac{k_\Delta}{2M_\Delta} \frac{G_C^*}{G_M^*} = \frac{\sqrt{2}S_{1/2}}{A_{1/2} + \sqrt{3}A_{3/2}}. \quad (12)$$

Here we use a definition for the G_C^* form factor, which is now mostly used in the literature. It differs from our previous definition [25] by a factor of $k_\Delta/2M_\Delta$.

In Fig. 3 we show our MAID2005 solution which can also be evaluated with the definitions of Eq. (8) and numerical numbers given in Table 1. The curves are compared to R_{EM} and R_{SM} ratios determined in different experimental analyses from MAMI, ELSA, Bates and JLab. The points at the two largest Q^2 values of 2.8 and 4.0 GeV^2 have been re-analyzed by our group [12]. Especially our R_{EM} values are more positive than in the original experimental analysis of Frolov et al. [20], which was done in a truncated multipole expansion. Also at $Q^2 = 1.0 \text{ GeV}^2$ we have performed such a re-analysis with the data of Kelly et al. [27] and also find an E/M ratio closer to our global solution. In this case, however, the data set is almost complete and consists out of 16 different polarization observables. But, of course also for this data set the angular resolution is limited and the observables have sizable errors in some cases. Therefore, we also find for this analysis a model uncertainty due to higher partial waves. In Fig. 4 we have enlarged

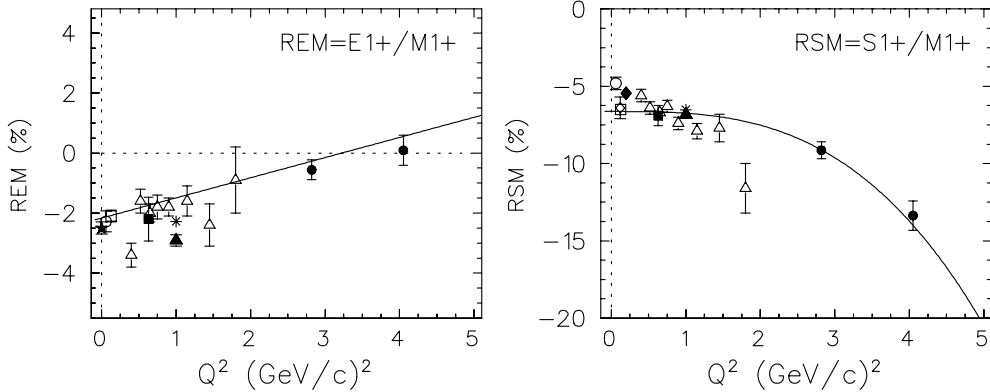


FIGURE 3. R_{EM} and R_{SM} ratios of the $\Delta(1232)$ resonance excitation at large Q^2 . The solid curves are the MAID2005 solutions. The experimental analyses are from: MAMI(solid star[9], open circles[29], open diamond[15], solid diamond [32]), Bates(open squares[16]), ELSA(solid squares[17]), JLab(open triangles[26], solid triangles[28]). The solid circles and asterisks show our own analysis to the JLab Hall C data[20] and JLab Hall A data[27], respectively.

the low Q^2 region, where the most recent experimental analysis from MAMI and Bates are shown. We note that in this region also preliminary data of CLAS have been analyzed and reported elsewhere in this proceedings [30]. Our global MAID solution which is practically constant in this Q^2 region is completely consistent with the individual data points of R_{EM} but does not have the right shape for R_{SM} . It was reported many times previously that in dynamical models R_{SM} has a tendency to rise and this was attributed to the pion cloud effects. In a dynamical calculation such a behavior arises naturally, in MAID, where the transition amplitudes are empirically parameterized, it has to be included by hand. As pointed out in more detail in Ref. [31] an important property is the model-independent behavior of the multipoles at physical threshold (vanishing pion momentum, $q = |\vec{q}| = 0$) and at pseudothreshold (Siegert limit, vanishing photon momentum $k = |\vec{k}| = 0$). In particular we find the following conditions for the Delta multipoles: $(E_{1+}, M_{1+}, L_{1+}) \rightarrow kq$. Due to gauge invariance, $kL_{1+} = \omega S_{1+}$, the Coulomb amplitudes acquire an additional factor k at pseudothreshold, i.e., $S_{1+} \sim kL_{1+}$. The Siegert limit is reached at $Q^2 = Q_{pt}^2 = -(W - M_N)^2$, and since $\vec{k} = 0$ means that no direction is defined, the electric and longitudinal multipoles have to be equal at this point, $L_{1+}(Q_{pt}^2) = E_{1+}(Q_{pt}^2)$

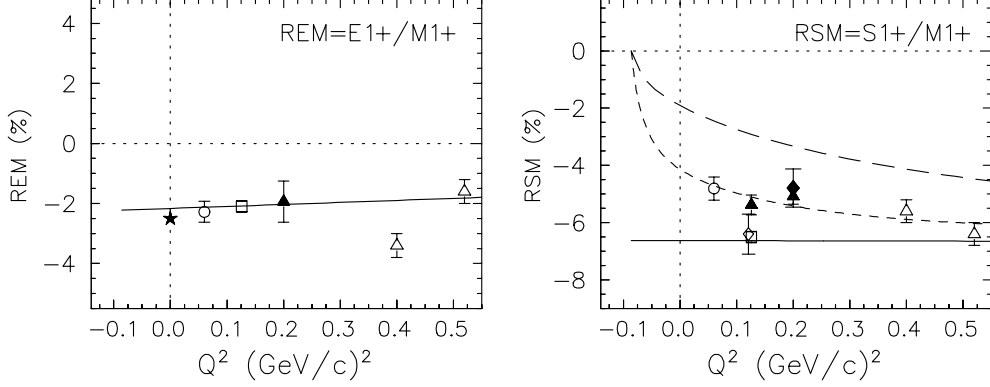


FIGURE 4. R_{EM} and R_{SM} ratios of the Δ excitation at low Q^2 . The solid triangles show a preliminary analysis with MAMI data at $Q^2 = 0.2 \text{ GeV}^2$ and a combined analysis of Bates and MAMI data at $Q^2 = 0.127 \text{ GeV}^2$ [33], all other experimental analyses are as in the previous figure. The solid curves are the MAID2005 solutions, whereas the dashed curves show two solutions that are consistent with the Siegert theorem at pseudothreshold, see text.

and $S_{1+}(Q_{pt}^2) = k/\omega E_{1+}(Q_{pt}^2)$. For the ratios at $W = M_\Delta$, we do not get a further constraint for R_{EM} , it remains finite at Q_{pt}^2 , but for R_{SM} we get the important condition

$$R_{SM} = \frac{S_{1+}}{M_{1+}} = \frac{k_\Delta}{\omega_\Delta} \frac{L_{1+}}{M_{1+}} = \frac{k_\Delta}{\omega_\Delta} \frac{E_{1+}}{M_{1+}} = \frac{k_\Delta}{M_\Delta - M_N} R_{EM}, \quad \text{for } k_\Delta \rightarrow 0. \quad (13)$$

This Siegert approximation is shown as the long-dashed line in Fig. 4. In this simplest form it looks very similar to the dynamical calculation of Sato and Lee [34, 35]. With further moderate adjustments in the Q^2 shape the empirical MAID parametrization can be improved to get a perfect fit through the data points (short-dashed line). However, this preliminary result is only a fit of the single- Q^2 points and not yet a fit to the measured cross sections.

In a recent paper of Elsner et al. [32] we have analyzed the longitudinal-transverse asymmetries LT and LT' measured at Mainz in two different experiments at $W = 1232 \text{ MeV}$ and $Q^2 = 0.2 \text{ GeV}^2$. These asymmetries are related to the partial cross sections via

$$\rho_{LT}(\theta) = \frac{\sqrt{2\varepsilon(1+\varepsilon)}d\sigma_{LT}}{d\sigma_T + \varepsilon d\sigma_L + \varepsilon d\sigma_{TT}} \quad \text{and} \quad \rho_{LT'}(\theta, \phi) = \frac{\sqrt{2\varepsilon(1-\varepsilon)}d\sigma_{LT'} \sin \phi}{d\sigma_T + \varepsilon d\sigma_L + \varepsilon d\sigma_{LT} \cos \phi + \varepsilon d\sigma_{TT} \cos 2\phi}. \quad (14)$$

The sensitivity to the leading multipoles M_{1+} , S_{1+} and S_{0+} is shown by a partial wave decomposition, where only the leading multipoles are retained,

$$\begin{aligned} \rho_{LT}(\theta) &\simeq f1(\theta) \frac{\Re\{(S_{0+} + 6S_{1+} \cos \theta)M_{1+}^*\}}{|M_{1+}|^2}, \\ \rho_{LT'}(\theta, \phi) &\simeq f2(\theta, \phi) \sin \phi \frac{\Im\{(S_{0+} + 6S_{1+} \cos \theta)M_{1+}^*\}}{|M_{1+}|^2}. \end{aligned} \quad (15)$$

At the resonance position, the P_{33} multipoles become purely imaginary, therefore, ρ_{LT} which is proportional to the real part of the product becomes very sensitive to the Delta resonance, whereas the imaginary part of the bilinear products in $\rho_{LT'}$ show up with an enhanced sensitivity to the background multipoles. Such background multipoles as S_{0+} for isospin 1/2 and 3/2 and S_{1+} for isospin 1/2 are not so well described within the unitary isobar model MAID. Only via PS-PV mixing, the vector meson contributions and the unitarization procedure they can get non-Born contributions. However, all these parameters are practically fixed, therefore we have allowed for an additional variation of a real and imaginary non-Born part in the S_{0+} multipole.

Using the new ρ_{LT} data of Elsner [32] in conjunction with the previous measurement of the $\rho_{LT'}$ asymmetry of Bartsch et al. [36], we performed a re-fit of the MAID2003 parameters. We obtained sensitivity to real and imaginary parts of the S_{1+} and S_{0+} amplitudes in the $p\pi^0$ channel. The results for ρ_{LT} and $\rho_{LT'}$ are depicted in Fig. 5, in comparison with the standard MAID2003 and the dynamical models DMT2001 [11, 12] and SL2001 [35]. Our MAID2003 re-fit results are also compared with a truncated analysis of Eq. (15) using only the 3 partial waves S_{1+} ,

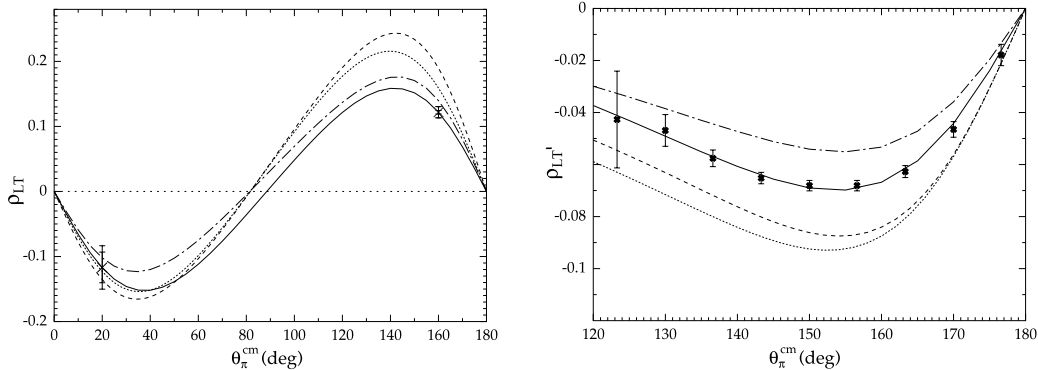


FIGURE 5. Left: ρ_{LT} asymmetries compared with model predictions from MAID2003 [14] (dotted), DMT2001 [11, 12] (dashed), Sato/Lee [35] (dashed dotted). The full curve represents the MAID2003 re-fit. Right: $\rho_{LT'}$ asymmetries from reference [36] with model predictions from MAID2003 [14] (dotted), DMT2001 [11, 12] (dashed), Sato/Lee [35] (dashed dotted). The full curve represents the MAID2003 re-fit.

S_{0+} and M_{1+} and with previous calculations in Table 2 as multipole ratios for the $(p\pi^0)$ channel. The denoted errors are due to the re-fit of S_{1+} and S_{0+} within the MAID2003 analysis taking into account the statistical and systematical errors. The model dependence of the extraction can be estimated from the truncated multipole result given in the second row in the table.

TABLE 2. Comparison of multipole ratios from asymmetry data and calculations, as discussed in the text.

	$\frac{\Re\{S_{1+}M_{1+}^*\}}{ M_{1+} ^2}$ (%)	$\frac{\Im\{S_{1+}M_{1+}^*\}}{ M_{1+} ^2}$ (%)	$\frac{\Re\{S_{0+}M_{1+}^*\}}{ M_{1+} ^2}$ (%)	$\frac{\Im\{S_{0+}M_{1+}^*\}}{ M_{1+} ^2}$ (%)
MAID2003 re-fit	-5.45 ± 0.42	-2.92 ± 0.48	2.56 ± 2.25	3.67 ± 2.33
from Eq. (15)	-4.78 ± 0.69	–	0.56 ± 3.89	–
MAID2003	-6.65	-2.22	7.98	15.0
DMT 2001	-6.81	-2.20	7.33	12.4
SL 2001	-4.74	-1.77	5.14	4.35

A comparison between the MAID2003 re-fit and the truncated result shows agreement for the S/M ratio (first column of Table 2). In general, however, the truncation can lead to wrong results as for the real part of the S_{0+}/M_{1+} ratio, but the large error takes account of this problem. The truncation in $\rho_{LT'}$ is even worse and would lead to completely wrong results for the imaginary parts of the ratios, therefore, we have omitted these numbers in the table. The biggest effect of our re-fit is observed in the imaginary part of S_{0+}/M_{1+} , which is reduced by a factor of 4 compared to the standard MAID calculation. This result shows the importance of non-Born terms in the background amplitude S_{0+} due to the pion cloud effects. Our fitted result is in good agreement with the dynamical model of Sato/Lee but in disagreement with the DMT model.

PHOTOCOUPPLING AMPLITUDES

Besides our extensive studies of the $\Delta(1232)$ resonance, we have also investigated the Q^2 evolution of all other resonance excitations that are included in MAID. At higher energies, above the Δ region, however, the data are no longer so abundant as in the Δ region, but due to a large data set of the CLAS collaboration [26, 19] for $p(e, e'\pi^0)p$ we were able to determine the transverse and longitudinal helicity photon couplings as functions of Q^2 for all 4-star resonances below 1700 MeV. The data are available in the kinematical region of $1100 \text{ MeV} < W < 1680 \text{ MeV}$ and $0.4 \text{ GeV}^2 < Q^2 < 1.8 \text{ GeV}^2$.

Above the 2π threshold the two-channel unitarity and consequently the Watson theorem no longer hold. Therefore, the background amplitude (Eq. (6)) of any partial wave α does not vanish at the resonance position, except for the $P_{33}(1232)$. This leads naturally to a model dependence in the resonance-background separation. Here in our analysis we use the concept of the MAID model, where the background and resonance contributions are already separated

according to the K-matrix approximation, Eqs. (5,6). Therefore, we can start with Eq. (7) for a general definition of the photon coupling amplitudes (see also PDG94 or Ref. [22]). At the resonance position, $W = M_R$ we then obtain

$$\begin{aligned}\mathcal{A}_\alpha^R(M_R, Q^2) &= i\bar{\mathcal{A}}_\alpha^R(Q^2)f_{\gamma R}(M_R)f_{\pi R}(M_R)c_{\pi R}e^{i\phi(M_R)} \\ &= \mathcal{A}_\alpha^{res}(M_R, Q^2)e^{i\phi(M_R)}\end{aligned}\quad (16)$$

with $f_{\gamma R}(M_R) = 1$ and

$$f_{\pi R}(M_R) = \left[\frac{1}{(2j+1)\pi} \frac{k_W}{|q|} \frac{M_N}{M_R} \frac{\Gamma_{\pi N}}{\Gamma_{tot}^2} \right]^{1/2}. \quad (17)$$

The factor $c_{\pi R}$ is $\sqrt{3/2}$ and $-1/\sqrt{3}$ for the isospin 3/2 and isospin 1/2 multipoles, respectively. This leads to the definition

$$\bar{\mathcal{A}}_\alpha^R(Q^2) = \frac{1}{c_{\pi R}f_{\pi R}(M_R)} \text{Im}\mathcal{A}_\alpha^{res}(M_R, Q^2). \quad (18)$$

It is important to note that by this definition the phase factor $e^{i\phi}$ in Eqs. (7) and (16) is not part of the resonant amplitude but rather part of the unitarization procedure. In the case of the $\Delta(1232)$ resonance this phase vanishes at the resonance position due to Watson's theorem, however, for all other resonances it is finite and in some extreme cases it can reach values of about 60° . $\bar{\mathcal{A}}_\alpha^R$ is a short-hand notation for the electric, magnetic and longitudinal multipole photon couplings of a given partial wave α . As an example, for the P_{33} partial wave the specific couplings are denoted by \bar{E}_{1+} , \bar{M}_{1+} and \bar{S}_{1+} . By linear combinations they are connected with the more commonly used helicity photon couplings $A_{1/2}$, $A_{3/2}$ and $S_{1/2}$. For resonances with total spin $j = \ell + 1/2$ we get

$$\begin{aligned}A_{1/2}^{\ell+} &= -\frac{1}{2}[(\ell+2)\bar{E}_{\ell+} + \ell\bar{M}_{\ell+}], \\ A_{3/2}^{\ell+} &= \frac{1}{2}\sqrt{\ell(\ell+2)}(\bar{E}_{\ell+} - \bar{M}_{\ell+}), \\ S_{1/2}^{\ell+} &= -\frac{\ell+1}{\sqrt{2}}\bar{S}_{\ell+}\end{aligned}\quad (19)$$

and for $j = (\ell + 1) - 1/2$

$$\begin{aligned}A_{1/2}^{(\ell+1)-} &= \frac{1}{2}[(\ell+2)\bar{M}_{(\ell+1)-} - \ell\bar{E}_{(\ell+1)-}], \\ A_{3/2}^{(\ell+1)-} &= -\frac{1}{2}\sqrt{\ell(\ell+2)}(\bar{E}_{(\ell+1)-} + \bar{M}_{(\ell+1)-}), \\ S_{1/2}^{(\ell+1)-} &= -\frac{\ell+1}{\sqrt{2}}\bar{S}_{(\ell+1)-}.\end{aligned}\quad (20)$$

In Fig. 6 we show our results for the $\Delta(1232)$, the $D_{13}(1520)$ and the $F_{15}(1680)$ resonances. Our superglobal fit agrees very well with our single- Q^2 fits, except in the case of the Δ resonance for the 2 lowest points of $S_{1/2}$ from our analysis of the Hall B data. As we discussed before, this is due to the wrong Siegert limit in MAID2005 for the longitudinal couplings, which will be corrected in the next version of MAID. It will also have consequences for higher resonances, however, the pseudothreshold at resonance energy moves further away from the physical region (e.g. $Q_{pt}^2 = -0.338 \text{ GeV}^2$ for the $D_{13}(1520)$) and will not have such a large consequence as in the case of the $\Delta(1232)$.

Our results for the spin 1/2 resonances $P_{11}(1440)$ and $S_{11}(1535)$ are shown in Fig. 7. As in the previous figure, our superglobal solutions are in a generally good agreement with our single- Q^2 points (triangles and circles). In this figure we also compare with the results of Aznauryan [37] using a similar data set of CLAS data. Both of our analyses are in good agreement, and furthermore, the overall fluctuation of the points give a realistic estimate of the model uncertainty. For the Roper resonance we notice a zero crossing of the transverse helicity coupling around $Q^2 \approx 0.7 \text{ GeV}^2$ and a maximum at a relatively large momentum transfer of 2.5 GeV^2 . Also the longitudinal Roper excitation exhibits very large values around $Q^2 \approx 0.5 \text{ GeV}^2$, in fact this is the strongest longitudinal resonance excitation that we can find. This should be a clear answer to the question raised by Li and Burkert [38], whether the Roper resonance is a radially excited 3-quark state or a quark-gluon hybrid state. In the latter case it was argued that the longitudinal coupling would completely vanish. Also the couplings of the $S_{11}(1535)$ resonance are quite strong. As it is already known from

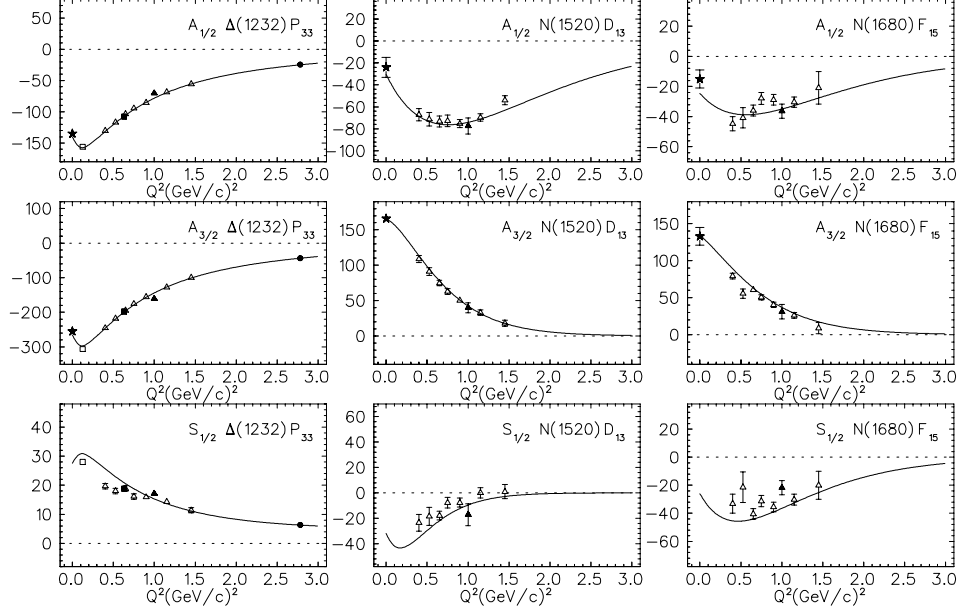


FIGURE 6. The Q^2 dependence of the transverse ($A_{1/2}, A_{3/2}$) and longitudinal ($S_{1/2}$) helicity couplings for the $P_{33}(1232)$, $D_{13}(1520)$ and $F_{15}(1680)$ resonance excitation. The solid curves show our superglobal fit. The data points at finite Q^2 are obtained from our single- Q^2 analysis using the data from MAMI and Bates for $Q^2 = 0.1 \text{ GeV}^2$, from ELSA for 0.6 GeV^2 , JLAB(Hall A) for 1.0 GeV^2 , JLab(Hall C) for 2.8 GeV^2 and JLab(Hall B) for the remaining points. At the photon point ($Q^2 = 0$) we show our result of the photoproduction analysis.

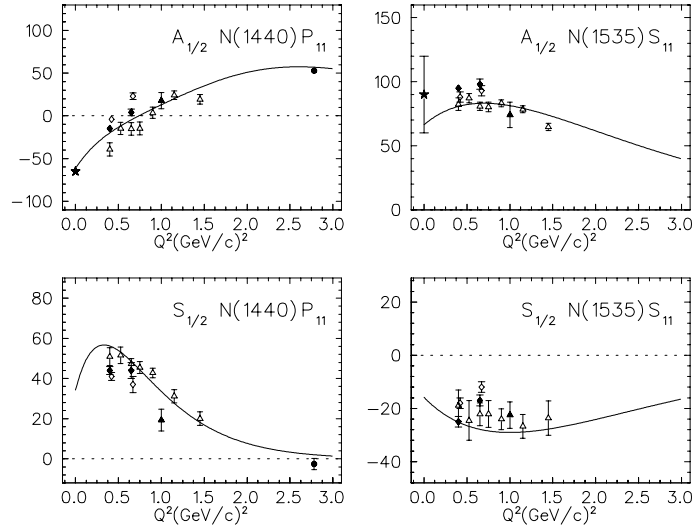


FIGURE 7. The Q^2 dependence of the transverse and longitudinal helicity amplitudes for the $P_{11}(1440)$ and the $S_{11}(1535)$ resonance excitation of the proton. The solid lines are the superglobal Maid2005 solutions. The solid red (gray) points are our single- Q^2 fits to the exp. data from CLAS/JLab [19], the solid and open blue circles show the isobar and dispersion analysis of Aznauryan [37] using a similar data set.

η electroproduction, the transverse form factor falls off very weakly. At $Q^2 \approx 3 \text{ GeV}^2$ it is much stronger than the Delta or the D_{13} and is comparable to the Roper. However, due to the much smaller width of the S_{11} compared to the Roper, the resonant amplitude (see Eq. (16)) of the S_{11} dominates at large Q^2 . This result is in agreement with the observation in the inclusive electroproduction cross section of the proton, where at small momentum transfer the $\Delta(1232)$ dominates but at large momentum transfer the second resonance region takes over.

CONCLUSIONS

Using the world data base of pion photo- and electroproduction and recent data from Mainz, Bonn, Bates and JLab we have made a first attempt to extract all longitudinal and transverse helicity amplitudes of nucleon resonance excitation for four star resonances below $W = 1.7$ GeV. For this purpose we have extended our unitary isobar model MAID and have parameterized the Q^2 dependence of the transition amplitudes. Comparisons between single- Q^2 fits and a Q^2 dependent superglobal fit give us confidence in the determination of the helicity couplings of the $P_{33}(1232)$, $P_{11}(1440)$, $S_{11}(1535)$, $D_{13}(1520)$ and the $F_{15}(1680)$ resonances, even though the model uncertainty of these amplitudes can be as large as 50% for the longitudinal amplitudes of the D_{13} and F_{15} .

For other resonances the situation is more uncertain. However, this only reflects the fact that precise data in a large kinematical range are absolutely necessary. In some cases double polarization experiments are very helpful as has already been shown in pion photoproduction. Furthermore, without charged pion electroproduction, some ambiguities between partial waves that differ only in isospin as S_{11} and S_{31} cannot be resolved without additional assumptions. While all electroproduction results discussed here are only for the proton target, we have also started an analysis for the neutron, where much less data are available from the world data base and no new data has been analyzed in recent years. Since we can very well rely on isospin symmetry, only the electromagnetic couplings of the neutron resonances with isospin 1/2 have to be determined. We have obtained a superglobal solution for the neutron which is implemented in MAID2005. However, for most resonances this is still highly uncertain. So it will be a challenge for the experiment to investigate also the neutron resonances in the near future.

ACKNOWLEDGMENTS

This work was supported in part by the Deutsche Forschungsgemeinschaft (SFB443).

REFERENCES

1. G. Höhler *et al.*, Handbook of Pion-Nucleon Scattering, Physics Data 12-1 (Karlsruhe, 1979).
2. S. Eidelman *et al.* (Particle Data Group), Phys. Lett. B 592 (2004) 1.
3. N. Kaiser, P.B. Siegel and W. Weise, Nucl. Phys. A 594 (1995) 325; N. Kaiser, T. Waas and W. Weise, Nucl. Phys. A 612 (1997) 297.
4. O. Krehl, C. Hanhart, S. Krewald and J. Speth, Phys. Rev. C 62 (2000) 025207.
5. E.E. Kolomeitsev and M.F.M. Lutz, Phys. Lett. B 585 (2004) 243.
6. S.J. Dong, T. Draper, I. Horvath, F.X. Lee, K.F. Liu, N. Mathur and J.B. Zhang, hep-ph/0306199; F.X. Lee and C. Bennhold, Nucl. Phys. A 754 (2005) 248.
7. C. Alexandrou *et al.*, Phys. Rev. Lett. 94 (2005) 021601.
8. For an overview and further references see S. Boffi, C. Giusti, F.D. Pacati and M. Radici, Electromagnetic Response of Atomic Nuclei, Clarendon Press, Oxford, 1996, p. 114ff.
9. R. Beck *et al.*, Phys. Rev. Lett. 78 (1997) 606 and Phys. Rev. C 61 (2000) 035204.
10. S.N. Yang, J. Phys. G 11 (1985) L205.
11. S.S. Kamalov and S.N. Yang, Phys. Rev. Lett. 83 (1999) 4494.
12. S.S. Kamalov, S.N. Yang, D. Drechsel, O. Hanstein and L. Tiator, Phys. Rev. C 64 (2001) 032201.
13. G.-Y. Chen, S. Kamalov, S.N. Yang, D. Drechsel and L. Tiator, Nucl. Phys. A 723 (2003) 447.
14. D. Drechsel, O. Hanstein, S.S. Kamalov and L. Tiator, Nucl. Phys. A 645 (1999) 145; <http://www.kph.uni-mainz.de/MAID/>.
15. Th. Pospischil *et al.*, Phys. Rev. Lett. 86 (2001) 2959.
16. C. Mertz *et al.*, Phys. Rev. Lett. 86 (2001) 2963.
17. T. Bantes, PhD thesis Bonn 2003, BONN-IR-2003-08.
18. G. Laveissiere *et al.*, Phys. Rev. C 69 (2004) 045203.
19. L.C. Smith, private communication.
20. V.V. Frolov *et al.*, Phys. Rev. Lett. 82 (1999) 45.
21. R.A. Arndt, W.J. Briscoe, I.I. Strakovsky and R.L. Workman, Phys. Rev. C 66 (2002) 055213; <http://gwdac.phys.gwu.edu/>.
22. R.A. Arndt, R.L. Workman, Z. Li and L.D. Roper, Phys. Rev. C 42 (1990) 1864.
23. W.W. Ash *et al.*, Phys. Lett. B 24 (1967) 165.
24. H.F. Jones and M.D. Scadron, Annals Phys. 81 (1973) 1.
25. L. Tiator, D. Drechsel, S.S. Kamalov and S.N. Yang, Eur. Phys. J. A 17 (2003) 357.
26. K. Joo *et al.*, (CLAS collaboration), Phys. Rev. Lett. 88 (2002) 122001.
27. J.J. Kelly *et al.*, Phys. Rev. Lett. 95 (2005) 102001 and nucl-ex/0509004.
28. J.J. Kelly, Phys. Rev. C 72 (2005) 048201.

29. S. Stave *et al.* (A1 collaboration), nucl-ex/0604013.
30. L.C. Smith, Contribution to this Proceedings.
31. D. Drechsel and L. Tiator, Contribution to this Proceedings.
32. D. Elsner *et al.*, Eur. Phys. J. A 27 (2006) 91.
33. N.F. Sparveris, Contribution to this Proceedings.
34. T. Sato and T.S.H. Lee, Phys. Rev. C 54 (1996) 2660.
35. T. Sato and T.S.H. Lee, Phys. Rev. C 63 (2001) 055201.
36. P. Bartsch *et al.*, Phys. Rev. Lett. 88 (2002) 142001.
37. I. Aznauryan, V. Burkert, H. Egiyan, K. Joo, R. Minehart and L.C. Smith, Phys. Rev. C 71 (2005) 015201.
38. Z. Li, V. Burkert and Z. Li, Phys. Rev. D 46 (1992) 70.